nature physics

SUPPLEMENTARY INFORMATION

DOI: 10.1038/NPHYS1999

# Quantum control of proximal spins using nanoscale magnetic resonance imaging

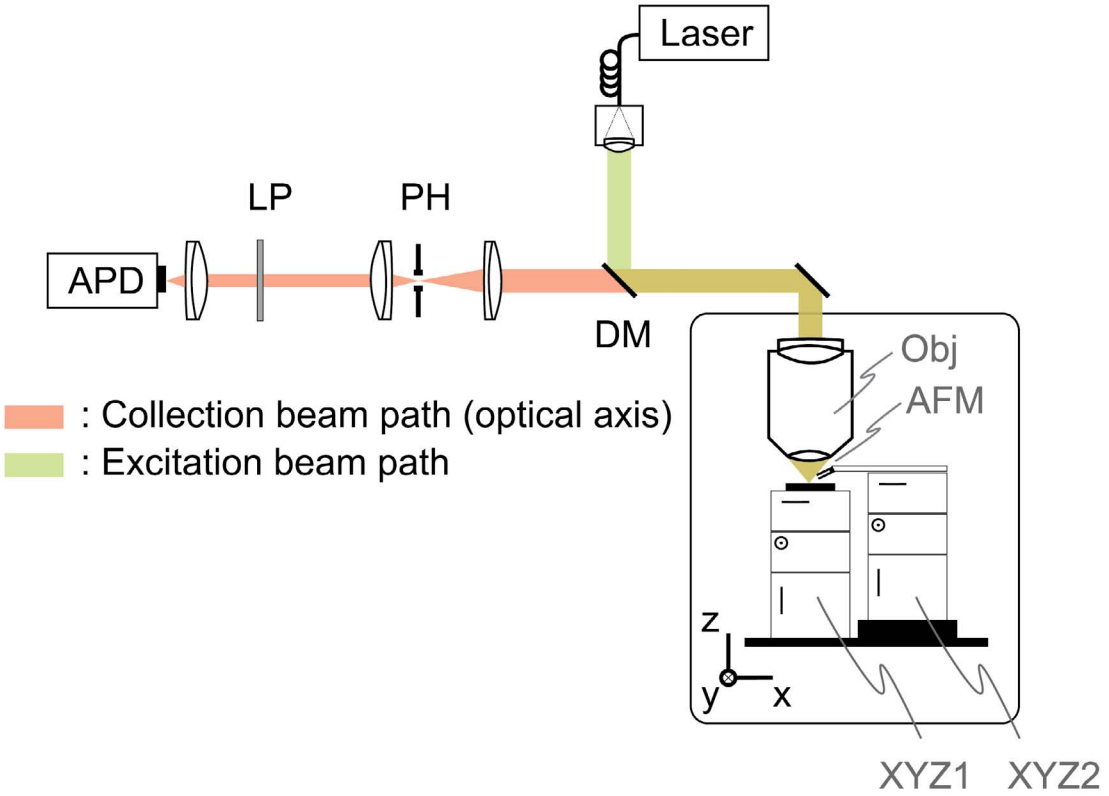



**Figure S1:** Combined AFM and confocal microscope. Two stacks of piezo coarse positioners and scanners (Attocube ANPxyz101/RES and ANSxyz100) are used for positioning a magnetic tip and a bulk diamond sample containing NV centers. NV centers are placed at the focus of a confocal microscope using one set of piezo scanners (XYZ1), while the tip's distance to the sample is regulated via AFM feedback on the other set of stacks (XYZ2). Atomic force detection is done electrically by measuring changes in the resonant frequency of an oscillating tuning-fork operating in shear mode. The tip can be scanned using XYZ2 to produce magnetic resonance images, while NV spins on the sample are read out confocally. A green excitation laser (532 nm wavelength) is focued on the NV centers using a long working distance objective (Mitutoyo, M Plan Apo NI R 100sX) and excites NV centers non-resonantly, which then fluoresce at longer wavelengths. An acousto-optical modulator (not illustrated), is used to pulse the laser allowing for measuring the time-dependent fluorescence of NV centers. A dichroic mirror (DM) separates the collection and excitation laser paths to avoid unwanted photon counts from the excitation laser. Emitted light passes through a telescope containing a pinhole (PH), making the optical detection confocal. A longpass filter (LP) is used to further suppress green excitation counts before the emitted light is collected via an avalanche photo diode (APD) (Perkins and Elmer, SPCM-AQRH-13).

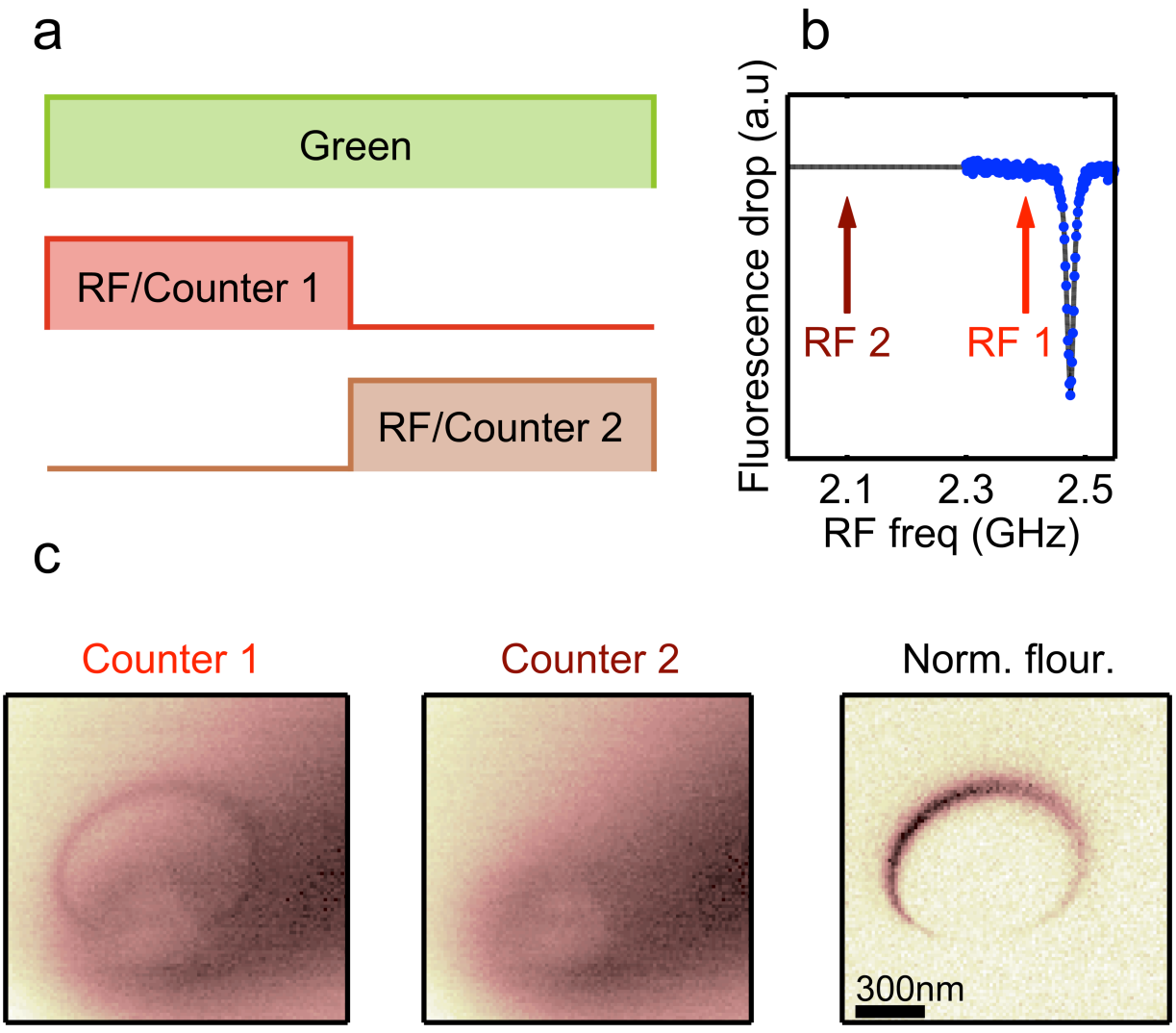



**Figure S2:** Normalized fluorescence for magnetic imaging. (a) Pulse sequence for magnetic resonance imaging. Green light is continuously applied to the NV center. For the first half of the sequence, one radio-frequency (RF 1) field is applied, and the corresponding NV counts are collected in counter 1. For the second half of the sequence, the same is done for RF 2 and counter 2. The length of the total sequence is roughly 50 us, much longer than the spin-pumping time and much shorter than the pixel integration time of our MRI scans. (b) The frequency of RF 1 is tuned close to the NV resonance, while RF 2 is detuned by more than 10 linewidths so that the tip never brings the NV spin into resonance with RF 2. (c) When a tip is scanned over the sample (same data as Figure 1c in the main text), counts are collected in both counter 1 and counter 2. Counter 1 contains a magnetic contour showing the location where the tip brings the NV into resonance with RF 1. However, there are also significant non-magnetic features due to artifacts such as tip shadowing and the influence of topographic features. These non-magnetic features can be removed by normalizing counter 1 to counter 2; the latter is affected by the same artifacts as the former but contains no magnetic signal. This normalization results in an image that has only magnetic-field induced fluorescence variations. We note that by modulating between two RF sources, the overall RF power can be kept constant in time, which is crucial for maintaining AFM performance

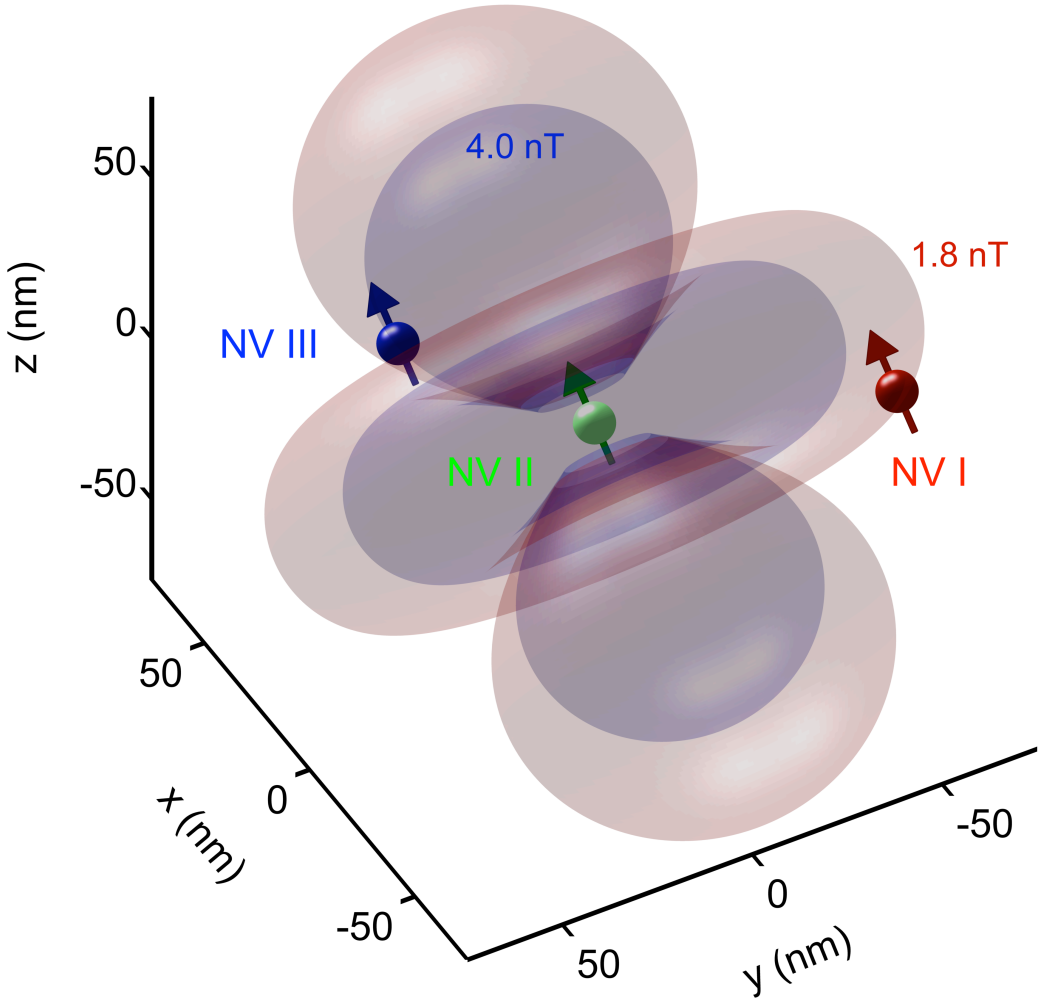



**Figure S3:** Theoretical NV dipole coupling for the measured NV locations. NV spin locations are plotted, as measured from magnetic resonance imaging (NVs I, II, and III, from Figure 2). Arrows indicate the NV orientation determined by measuring the Zeeman splitting along different directions with a three-axis Helmholtz coil (data not shown). All three NVs have the same NV axis. The dipolar magnetic field strength from NV II along the NV axis is plotted as a function of position. We plot equal field-strength contours that intersect NV I (red) and NV III (blue), yielding their theoretical dipolar coupling strengths of 1.8 nT and 4.0 nT respectively. The shapes of the contours indicate the strong angular dependence of the coupling strength, illustrating the importance of three-dimensional imaging for a priori determination of NV coupling frequencies. With the calculated dipole couplings, we can estimate the individual spin coherence times needed for the generation of entangled spin states. For the spins with 4.0 nT coupling, the corresponding dipole coupling rate is 110 Hz, indicating that a coherence time of 10 ms would be needed to achieve entanglement. The current literature best values of NV spin coherence is 1.8 ms[1], indicating if the distance between the imaged spins were reduced by a factor of two, and if these spins had equally long coherence times, spin-entanglement could be facilitated by our scanning magnetic field-gradient.

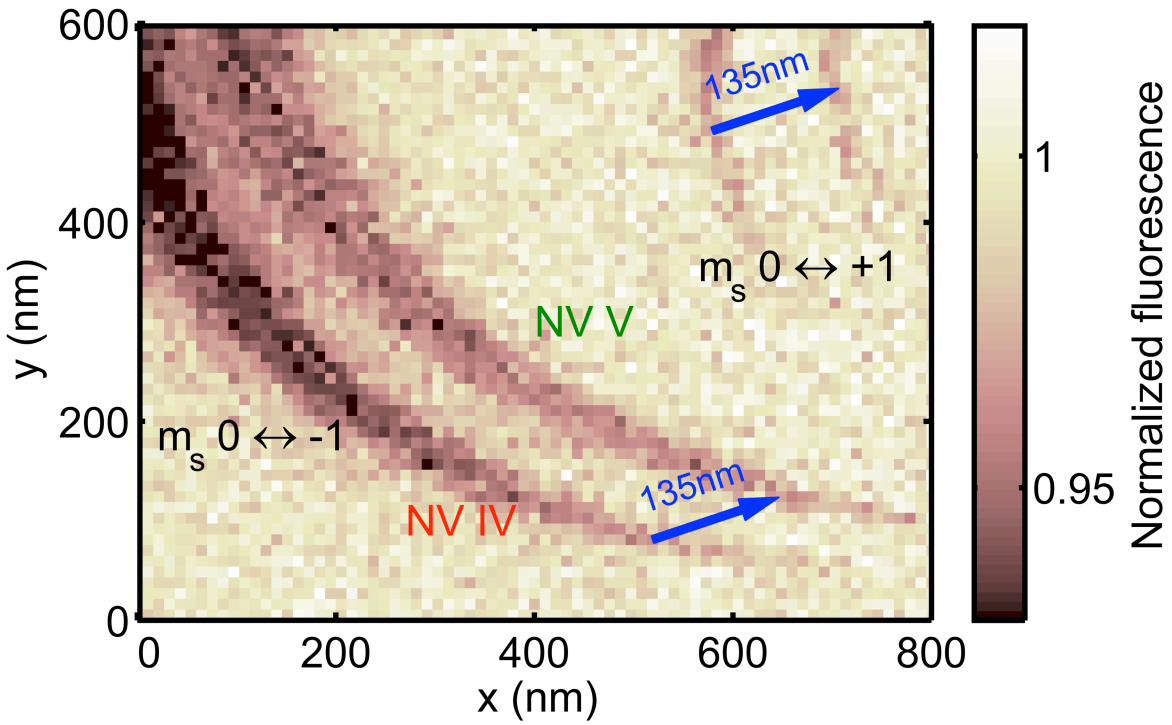



**Figure S4:** Distance between NV IV and NV V. Analogous to Figure 2, magnetic imaging is performed on NVs IV and V to determine their relative lateral distances. When the tip is scanned over of the pair of NVs, four contours are seen for the two NVs. There are two contours per NV because the tip field is strong compared to the applied static field, which splits the $m_S$=-1 and $m_S$=+1 in the NV triplet groundstate. Unlike the imaging done in Figures 1 and 2, where the tip is only strong enough to bring one spin transition into resonance, now the tip can bring either $m_S$=-1 or $m_S$=+1 into resonance with $m_S$=0, depending on the sign of the field. The distance between NVs is given by the spatial offset of the magnetic contours for the two NVs, which is the same for both spin transitions and is 135 nm (length of blue arrows). We note that this configuration of field-strength and detuning is advantageous in this situation, since the detection of the two ESR transitions ($m_S$=0 ↔ $m_S$=-1 and $m_S$=0 ↔ $m_S$=1) allows for accurately determining both x and y displacements of the NV centers while maintaining a small scan range.

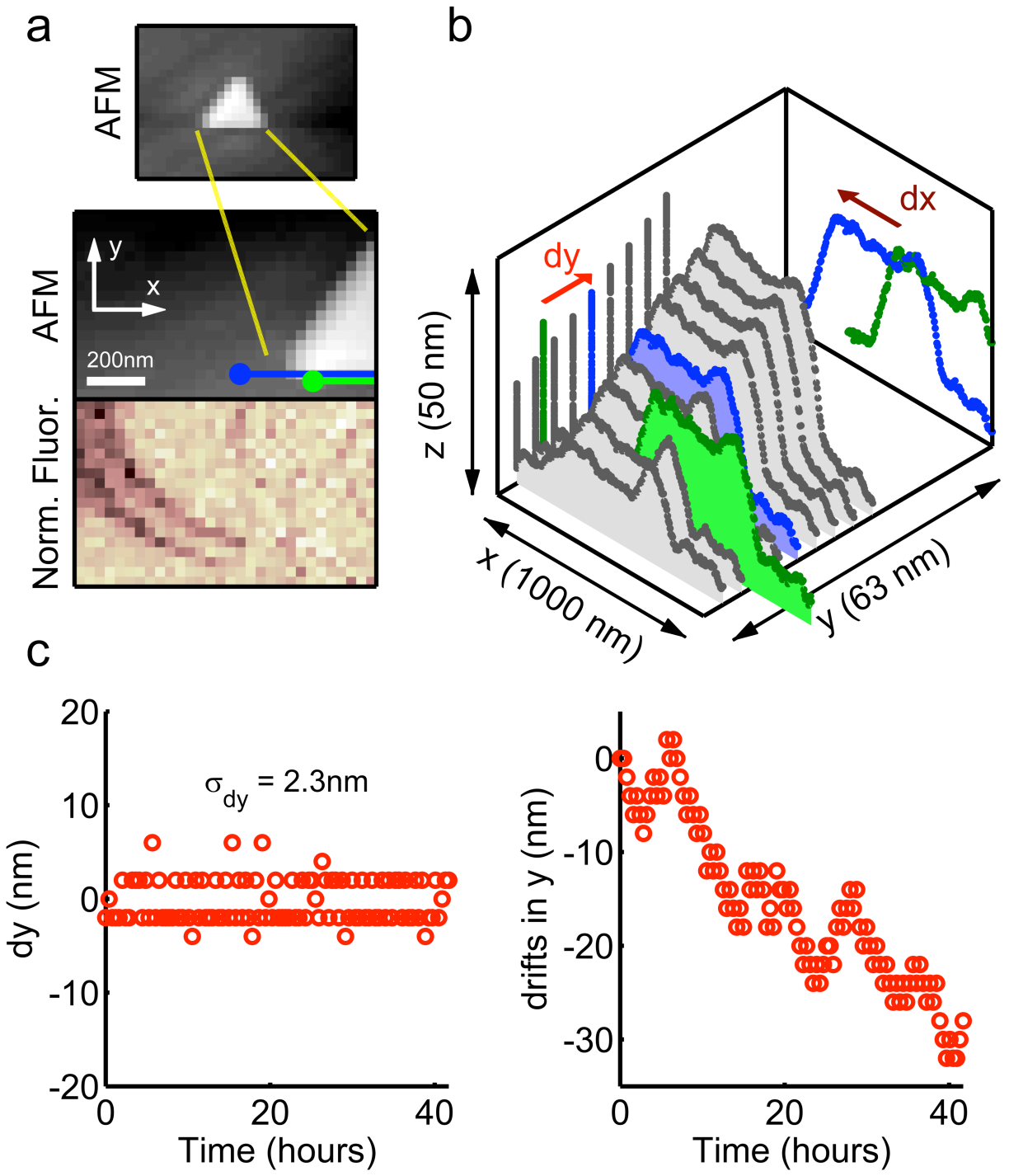



**Figure S5:** Active AFM drift correction. (a) AFM topographic image of an NV-containing nanostructure (here a triangle). This triangle contains the two NV centers studied in Figures 3 and 4 in the main text. Magnetic resonance imaging is performed on the two NV spins, and their magnetic responses are observed in the normalized fluorescence (plotted is the same region as Figure S4). In order to achieve coherent control of each of the two spins, it is necessary to position the tip where it splits the two NV resonances and maintain the tip location with few-nm

resolution to overcome NV spin-decoherence induced by tip-drifts. Here, we fix the tip at the green marker, but after performing experiments on each NV spin, the tip may have changed location due to temperature-induced drifts or piezo-electric creep. As an example of drifts, whose magnitude is exaggerated here, we examine the situation where the tip has drifted from the green marker to the blue marker. (b) Lateral positioning feedback via line-scan correction. The real-space location of the drifted tip is unknown. To determine its location efficiently, we take a single AFM line-scan which intersects the edge of the AFM triangular structure (green line in (a)). We plot the measured line-scan topography (green line), and cross-correlate it with individual lines of a topographic scan of the triangle edge (blue and grey lines). The AFM line yielding the highest cross-correlation (blue line), measures the tip's drift in the y-direction (dy). Drifts in the x-direction (dx) can additionally be extracted from the spatial offset between the green and blue panels, which is given by the location of the peak in the performed cross-correlation. (c) Lateral positioning feedback performance. Positioning is performed intermittently, and the resulting drifts in the y-direction (dy) are plotted (left panel). Magnetic field-gradients are predominantly directed along the y-direction (measured from the MRI image of the NVs in (a)), and consequently achieving high-precision in y-positioning is necessary for maintaining the NV spins resonance. Here we show positioning can be achieved with a standard deviation of 2.3 nm, only limited by pixelation of the topographic data. Spatial variations can then be converted to spectral uncertainties using the measured magnetic field gradient of our tip (0.1 G/nm here), indicating that the magnetic resonance can be maintained with 500 kHz precision. This sets a limit for tip-drift induced decoherence of NV spins which is smaller than the inhomogeneous dephasing rate ($1/T_2^*$) of the NV spins studied here. Integrating the measured drifts between line-scans gives the overall tip motion (right panel), which indicates that the tip location would drift considerably more without the use of line-scan feedback.

**Supplementary Discussion: Deconvolution to extract spin-spin distances**

A deconvolution process is used to extract the relative distance between NVs from the magnetic contours in Figure 2 of the main text. As the magnetic response of each NV spin to the tip is identical, but spatially shifted, we note that images of multiple NV spins are simply the magnetic response of one NV convolved with a map of delta functions corresponding to the spins' relative locations. Thus, we can use deconvolution of the observed magnetic image with the response of one of the NV spins to retrieve relative spin locations. Doing so requires the point spread function of a single NV spin, which can be found by first measuring the response of a single NV spin before moving to ensemble systems. Alternatively, for ensembles where there is not significant overlap between magnetic resonance curves, one can isolate a single ring and use that as the point-spread function for the deconvolution. We use the latter approach here by manually cropping out data not associated with NV II's magnetic resonance (the "single-spin response" shown in Figure 2a in the main text).

Once the point-spread function of a single spin is determined, deconvolution can be readily performed. Because of finite signal to noise ratios in our data, applying a filter during the deconvolution process is necessary to avoid artificial divergences. We accomplish this by using a Wiener filter, provided in the MATLAB Image Processing Toolbox, which minimizes the contribution from noise at frequencies which have low signal-to-noise ratios[2]. Optimal Wiener deconvolution filtering is dictated by the noise power spectrum of the image, and for NV spin states read out optically, the dominant source of noise is photon shot noise. Thus, the only relevant parameter is the signal to noise ratio of the image, which we find to be 7. Using this value yields the deconvolved image in Figure 2, which results in an image where each NV spin's location corresponds to a single peak. The deconvolved image is normalized such that the integrated intensity is equal to the number of imaged spins (3 in this case). This is chosen so that if the deconvolved image is convolved with the point spread function, each NV spin will have the correct fluorescence intensity.

An estimate for the precision in locating NV centers can be additionally extracted from the deconvolved image. This is achieved by performing a nonlinear regression fit of a two-dimensional Gaussian to the peak corresponding the NV spin of interest. From the covariance matrix of the errors, the uncertainty of the Gaussian peak position can be determined. This estimate only accounts for random, uncorrelated errors in the fitting, so for these measurements, this estimate is limited by photon shot noise in the NV spin readout and random drifts in the tip-to-sample distance. Here, with a pixel integration time of 7 s we achieve 0.2 nm precision. With the scan containing 100 x 100 pixels, this leads to an overall integration time of 19.1 hours. Such integration times are necessary because of low ESR contrast (~4%, due to imaging multiple spins and the presence of large off-axis fields) and moderate count rates (~34k counts per second, due to our 0.7 NA long working distance objective and low-laser power requirements from the magnetic tip).

In the performed imaging, we note that the peak corresponding to NV I is significantly skewed (as compared to NV III) because that NV lies at a different depth (15 nm further into the surface) than NV II, which slightly modifies its response to the magnetic tip. In principle, to deconvolve spins separated in three dimensions it is necessary to perform a deconvolution on the three-dimensional response of the NV spins to the tip. For this work, because spins are separated laterally more than in the z-direction, this is unnecessary for measuring relative spin distances.

Performing deconvolution is more involved if NV spins in an ensemble are not identically oriented. In bulk diamond, there are four possible quantization axes for NV centers, dictated by the crystallographic vector connecting the nitrogen atom and neighboring carbon vacancy. As spins' resonant frequencies predominantly shift to energies along their quantization axes, up to four different magnetic responses can be observed upon scanning arbitrary NV spin ensembles with a magnetic tip. While simple deconvolution can be used to find the relative distances

between spins sharing an axis in the ensemble, finding the relative distances between the four NV types requires additional consideration.

One method for measuring the distance between NV spins of different axes is to magnetize the tip-field to be perpendicular to the diamond surface, which for cylindrical tip geometries will yield a cylindrically symmetric magnetic field. Then for [0 0 1] diamond crystals, where all four NV axes have the same projection along the z-direction, the tip induces an identical, but rotated, magnetic response from each NV axis direction. Thus deconvolution can again be performed after rotating the magnetic response by 90, 180, or 270 degrees depending on the NV axis. Alternatively, for tips without cylindrical symmetry, the sample can be rotated in $90^{o}$ increments to have each NV direction respond identically to the tip. Relative distances between these four measurements can be determined by using AFM topography, which should not change upon rotation of the sample and can thus be used to correlate the magnetic measurements. Additionally, this technical challenge is unique to spins associated with NV centers, where the quantization is defined by a zero-field splitting along a crystallographic vector. For many other systems, the quantization axis for spins can be dictated by an externally applied field, and consequently all spins will respond identically to the local tip field.


1 Balasubramanian, G. *et al.* Ultralong spin coherence time in isotopically engineered diamond. *Nat Mater* **8**, 383-387 (2009).

2 Gonzalez, R. C. & Woods, R. E. *Digital Image Processing*. (Addison-Wesley Publishing Company, Inc., 1992).